





## Mass yields of fission fragments of Pt to Ra isotopes

Krzysztof Pomorski <sup>1</sup>, Artur Dobrowolski,<sup>1</sup> Rui Han <sup>1</sup>, Bożena Nerlo-Pomorska,<sup>1</sup> Michał Warda <sup>1</sup>, Zhigang Xiao,<sup>2</sup> Yongjing Chen,<sup>3</sup> Lilie Liu,<sup>3</sup> and Jun-Long Tian <sup>4</sup>

<sup>1</sup>*Institute of Physics, Maria Curie Skłodowska University, 20-031 Lublin, Poland*

<sup>2</sup>*Department of Physics, Tsinghua University, Beijing 100084, China*

<sup>3</sup>*China Institute of Atomic Energy, Beijing 102413, China*

<sup>4</sup>*School of Physics and Electrical Engineering, Anyang Normal University, Anyang 455000, China*



(Received 23 January 2020; revised manuscript received 1 April 2020; accepted 14 May 2020; published 2 June 2020)

An effective Fourier nuclear shape parametrization, which describes well the most relevant degrees of freedom on the way to fission is used to construct a three-dimensional collective model. The potential energy surface is evaluated within the macroscopic-microscopic approach based on the Lublin-Strasbourg drop macroscopic energy and Yukawa-folded single-particle potential. A phenomenological inertia parameter is used to describe the kinetic properties of the fissioning system. The fission fragment mass yields are obtained by using an approximate solution of the underlying Hamiltonian. The predicted mass fragmentations for even-even Pt to Ra isotopes are compared with available experimental data. Their main characteristics are well reproduced when the neck rupture probability dependent on the neck radius is introduced.

DOI: [10.1103/PhysRevC.101.064602](https://doi.org/10.1103/PhysRevC.101.064602)

### I. INTRODUCTION

A proper reproduction of the fission fragments mass distribution (FMD) is one of the most important tests of any theoretical model describing the nuclear fission process. A very nice review of the existing fission models can be found in Ref. [1], which is dedicated to the memory of Arnie J. Sierk, one of the leaders in this field of physics. Readers who are interested in the theory of nuclear fission can find more details in the textbook [2]. So we are not going to recall similar information here.

In the present paper we obtain such a distribution by an approximate solution of the eigenproblem of the three-dimensional (3D) collective Hamiltonian, which corresponds to the fission, neck, and mass-asymmetry modes, respectively. The nonadiabatic and dissipative effects in low-energy fission were taken into account in a similar way as in Refs. [3–6]. The potential energy surface (PES) is obtained by the macroscopic-microscopic (mac-mic) method, where the Lublin-Strasbourg drop (LSD) model [7] has been used for the macroscopic part of the energy, while the microscopic shell and pairing corrections have been evaluated through the Yukawa-folded (YF) single-particle levels [8,9]. The shape of the fissioning nucleus was described by the three-dimensional Fourier parametrization [10,11]. It was shown in Refs. [10,12] that this parametrization described very well the shapes of the nuclei even those close to the scission configuration.

The paper is organized in the following way. First we present briefly the details of the theoretical model, then we show the collective potential energy surface evaluated by the mac-mic model for the selected Pt to Ra isotopes. The calculated fission FMD's are compared with the existing

experimental data in the following section. Conclusions and plans of further calculations are presented in Sec. IV.

### II. MODEL OF THE FISSION DYNAMICS

The evolution of a nucleus from the equilibrium state towards fission is simulated by a simple dynamical approach based on the PES, which depends on three relevant collective degrees of freedom describing the nuclear shape in this process: elongation of the nucleus ( $q_2$ ), asymmetry of left and right mass fragments ( $q_3$ ), and the neck size ( $q_4$ ). As demonstrated in Refs. [10,11], the shape parametrization of the deformed nucleus, which gives an expansion of the nuclear surface in the form of the Fourier series of dimensionless coordinate  $(z - z_{sh})/z_0$ :

$$\frac{\rho_s(z)^2}{R_0^2} = \sum_{n=1}^{\infty} \left[ a_{2n} \cos\left(\frac{(2n-1)\pi}{2} \frac{z - z_{sh}}{z_0}\right) + a_{2n+1} \sin\left(\frac{2n\pi}{2} \frac{z - z_{sh}}{z_0}\right) \right] \quad (1)$$

is rapidly converging. As in the famous Funny-Hills parametrization [13],  $\rho_s(z)$  defines the distance of the surface point from the  $Oz$  symmetry axis, and  $z_0$  is the half-elongation of a nucleus between extreme points located at  $z_{\min} = z_{sh} - z_0$  and  $z_{\max} = z_{sh} + z_0$ . The quantity  $z_{sh}$  is responsible for shifting the center of mass of axially symmetric nuclear drop to be located at the origin of coordinate system.  $R_0$  represents the radius of the corresponding spherical nucleus of the same volume. In Eq. (1), the parameters  $a_2, a_3, a_4$  are related to the  $q_2, q_3, q_4$  deformation parameters through the following

formulas, respectively:

$$\begin{aligned} q_2 &= a_2^0/a_2 - a_2/a_2^0, \\ q_3 &= a_3, \\ q_4 &= a_4 + \sqrt{(q_2/9)^2 + (a_4^0)^2}, \\ q_5 &= a_5 - (q_2 - 2)\frac{a_3}{10}, \\ q_6 &= a_6 - \sqrt{(q_2/100)^2 + (a_6^0)^2}. \end{aligned} \quad (2)$$

These relations proposed in Ref. [11] transform the original deformation parameters  $a_i$  to the more natural parameters  $q_i$ , which ensure that only minor variations of the liquid drop fission paths occur around  $q_4 = 0$ . In addition, more and more elongated prolate shapes correspond to decreasing values of  $a_2$ , while oblate ones are described by  $a_2 > 1$ , which is in contradiction to the traditional definition of quadrupole deformation. Here  $a_n^{(0)}$  stands for the value of the  $a_n$  coefficient for a sphere:

$$a_{2n}^{(0)} = (-1)^{n-1} 32/[\pi (2n-1)]^3. \quad (3)$$

Having defined the shape parametrization of nuclear surface, one can now calculate the PES in 3D collective space. The nuclear deformation energies are determined in the macro approach, where the smooth energy part is given by the Lublin-Strasbourg drop (LSD) model [7] and the microscopic effects have been evaluated through a Yukawa-folded (YF) single-particle potential [8,9]. The Strutinsky shell-correction method [13–15] with a sixth-order correctional polynomial and a smearing width  $\gamma_S = 1.2\hbar\omega_0$  is used, where  $\hbar\omega_0 = 41/A^{1/3}$  MeV is the distance between the spherical harmonic-oscillator major shells. The BCS theory [16] with the approximate GCM+GOA-like particle number projection method [17] is used for the pairing correlations.

The pairing strengths  $G\mathcal{N}^{2/3} = 0.28\hbar\omega_0$ , with  $\mathcal{N} = Z, N$  for protons or neutrons, was adjusted to the experimentally measured mass differences of nuclei in this region with a pairing window containing  $2\sqrt{15\mathcal{N}}$  mean-field time-dependent degenerated levels lying around the Fermi level [18]. The mean field used to generate the single-particle energy levels, entering the Strutinsky and BCS quantum correction methods, is taken in the form of the folded Yukawa potential [8] and diagonalized in the deformed harmonic-oscillator basis with 18 major shells as written in Ref. [9].

The present research is a continuation and extension of our previous works [3–6]. The fundamental idea of the fission dynamics discussed in this work is that the relatively slow motion towards fission, mainly in  $q_2$  direction, is accompanied by the fast vibrations in the perpendicular  $q_3$  and  $q_4$  collective variables. This allows us to treat both of these two types of motion as decoupled, which, in consequence, gives the wave function corresponding to the total eigenvalue  $E$  of fissioning nucleus approximately as

$$\Psi_{nE}(q_2, q_3, q_4) = u_{nE}(q_2) \phi_n(q_3, q_4; q_2). \quad (4)$$

The function  $u_{nE}(q_2)$  is the eigenfunction corresponding to the motion towards fission, which depends mainly on a single variable  $q_2$ , while the  $\phi_n(q_3, q_4; q_2)$  simulates the  $n$ -phonon

fast collective vibrations on the perpendicular 2D  $\{q_3, q_4\}$  plane for a given elongation  $q_2$ .

There is a proper way to determine the  $u_{nE}(q_2)$  and  $\phi_n(q_3, q_4; q_2)$  wave function components in the discussed 3D collective space, respectively. For  $u_{nE}(q_2)$  one can use the WKB approximation for a single  $q_2$  mode as it has been done in Ref. [5], in which a 2D collective space has been considered, only. For  $\phi_n(q_3, q_4; q_2)$ , one can solve the eigenproblem of the underlying Hamiltonian in the perpendicular directions numerically. However, when limiting only to the low-energy fission, the density of probability  $W(q_3, q_4; q_2)$  of finding the system for a given elongation  $q_2$ , within the area of  $(q_3 \pm dq_3, q_4 \pm dq_4)$ , is given as

$$W(q_3, q_4; q_2) = |\Psi(q_2, q_3, q_4)|^2 = |\phi_0(q_3, q_4; q_2)|^2. \quad (5)$$

A further simplification of the model is to approximate the modulus square of the total wave function in Eq. (5) by the Wigner function in the form of

$$W(q_3, q_4; q_2) \propto \exp \frac{V(q_3, q_4; q_2) - V_{\min}(q_2)}{E_0}, \quad (6)$$

where  $V_{\min}(q_2)$  is the minimum of the potential for a given elongation  $q_2$ , and  $E_0$  is the zero-point energy, which is treated as an adjustable parameter.

To obtain the fragment mass yield for a given elongation  $q_2$  one has to integrate the probabilities (6) coming from different neck shapes, simulated basically by the  $q_4$  parameter

$$w(q_3; q_2) = \int W(q_3, q_4; q_2) dq_4. \quad (7)$$

It is clear that the fission probability may strongly depend on the neck thickness, strictly speaking, its radius  $R_{\text{neck}}$ . Following the idea from Ref. [5] one assumes the neck rupture probability  $P$  to be equal to

$$P(q_2, q_3, q_4) = \frac{k_0}{k} P_{\text{neck}}(R_{\text{neck}}), \quad (8)$$

where  $P_{\text{neck}}$  is a geometrical factor indicating the neck breaking probability proportional to the neck thickness, while  $k_0/k$  describes the fact that the larger collective velocity towards fission,  $v(q_2) = \dot{q}_2$ , gives the less probable neck rupture. The constant parameter  $k_0$  plays the role of scaling parameter, which is finally eliminated when calculating the resulting FMD. The expression for the geometrical probability factor  $P_{\text{neck}}(R_{\text{neck}})$  can be chosen in an arbitrary way to some extent, as, e.g., Fermi, Lorentz, and Gaussian functions [6]. In this paper, we used the Gaussian form as follows:

$$P_{\text{neck}}(R_{\text{neck}}) = \exp[-\log 2(R_{\text{neck}}/d)^2], \quad (9)$$

where  $d$  is the half-width of the probability, treated here as another adjustable parameter. The momentum  $k$  in Eq. (8) simulates the dynamics of the fission process, which, as usually, depends both on the local collective kinetic energy

$E - V(q_2)$  and the inertia towards the leading variable  $q_2$

$$\frac{\hbar^2 k^2}{2\bar{M}(q_2)} = E_{\text{kin}} = E - Q - V(q_2), \quad (10)$$

with  $\bar{M}(q_2)$  standing for the averaged inertia parameter over  $q_3$  and  $q_4$  degrees of freedom at a given elongation  $q_2$ , and  $V(q_2)$  is the averaged potential. In the further calculations we assume that the part of the total energy converted into heat  $Q$  is negligibly small due to the very low friction force when the collective velocity  $v(q_2)$  is small in low-energy fission. A good approximation of the inertia  $\bar{M}(q_2)$  is to use the irrotational flow mass parameter  $B_{\text{irr}}$  [19], which is derived initially as a function of the single collective parameter  $R_{12}$ , the distance between fragments, and the reduced mass  $\mu$  of both fragments

$$\bar{M}(q_2) = \mu[1 + 11.5(B_{\text{irr}}/\mu - 1)] \left( \frac{\partial R_{12}}{\partial q_2} \right)^2. \quad (11)$$

In order to make use of the neck rupture probability  $P(q_3, q_4; q_2)$  in Eq. (8), one has to rewrite the integral over  $q_4$  probability distribution (7) in the form of

$$w(q_3; q_2) = \int W(q_3, q_4; q_2) P(q_2, q_3, q_4) dq_4, \quad (12)$$

in which now the neck rupture probability is, in addition, taken into account. The above approximation implies a very important fact that, for a fixed  $q_3$  value, the fission may occur within a certain range of  $q_2$  deformations with different probabilities. Therefore, to obtain the true fission probability distribution  $w'(q_3; q_2)$  at a strictly given  $q_2$ , one has to exclude the fission events occurred in the previous  $q'_2 < q_2$  configurations, i.e.,

$$w'(q_3; q_2) = w(q_3; q_2) \frac{1 - \int_{q'_2 < q_2} w(q_3; q'_2) dq'_2}{\int w(q_3; q'_2) dq'_2}. \quad (13)$$

The normalized mass yield is then obtained as the sum of partial yields at different given  $q_2$ :

$$Y(q_3) = \frac{\int w'(q_3; q_2) dq_2}{\int w'(q_3; q_2) dq_3 dq_2}. \quad (14)$$

Since there is an one-to-one correspondence between  $q_3$  deformation and the masses of the left ( $A_L$ ) and right ( $A_R = A - A_L$ ) fission fragments, the yield function of Eq. (14) can be directly compared with the experimental FMD's now. One should notice that the scaling parameter  $k_0$  introduced in Eq. (8) does not longer appear in the definition of mass yield. Therefore, the only free parameters of the above model are zero-point energy parameter  $E_0$  in Eq. (5) and the half-width parameter  $d$  appearing in the probability of neck rupture (9).

In Ref. [6], the parameter  $d = 0.15R_0$  was adjusted to reproduce the experimental fragment mass yields measured in the low-energy fission of  $^{236-244}\text{Pu}$  isotopes. On the other hand, zero-point energy parameter  $E_0 = 1$  MeV related to the  $q_3$  and  $q_4$  degrees of freedom is kept constant. The comparison of the estimates obtained by the above model with the data taken from Ref. [20] is shown in Fig. 1. It can be seen that the agreement of this model predictions with the experimental yields is pretty good.

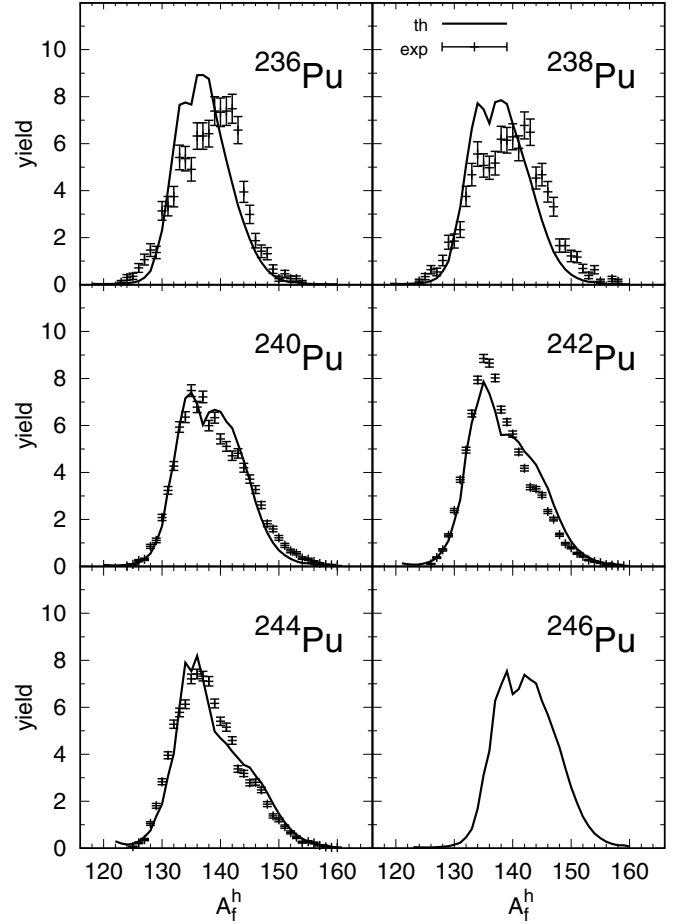


FIG. 1. Theoretical estimates (solid lines) of heavy fragment mass yield for fission of  $^{236-246}\text{Pu}$  isotopes compared with the experimental data (points with bars) from Ref. [20].

### III. RESULTS

The results obtained in Ref. [6] for Pu isotopes have encouraged us to investigate the possibilities of extending our model to predict/describe the FMD's of the low-energy fission of Hg, Pt, Pb, Po, Rn, and Ra nuclei. The fission barriers of these nuclei around  $^{208}\text{Pb}$  are significantly higher than those for actinides. In these nuclei a typical potential energy difference between the energies of the saddle and the most probable scission point is of the order of a few MeV, which is about only one order of magnitude smaller than that in actinides. It is then clear that in these two nuclear regions, the role of the fission dynamics should be significantly different.

The PES of all the considered nuclei are evaluated on the following 4D grid in the deformation parameter space (2):

$$\begin{aligned} q_2 &= -0.60(0.05)2.35, \\ q_3 &= 0.00(0.03)0.21, \\ q_4 &= -0.21(0.03)0.21, \\ \eta &= 0.00(0.03)0.21, \end{aligned} \quad (15)$$

where the parameter  $\eta$  describes the non-axial shapes of nuclei as defined in Ref. [11]. It turns out that for all the considered



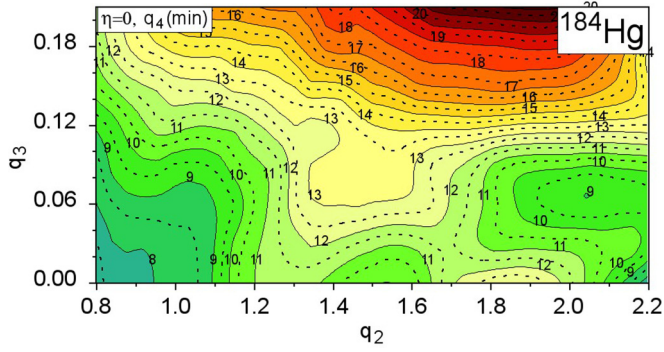


FIG. 2. Potential energy surface of  $^{184}\text{Hg}$  at the  $(q_2, q_3)$  plane minimized with respect to  $q_4$ .

isotopes  $\eta \neq 0$  may only appear in rather less elongated nuclei. Its influence practically ends around the deformations corresponding to the first saddle point in the fission barrier, i.e., at  $q_2 \approx 1.3$ . Since in the following we will only consider the fission fragment mass distribution of nonrotating nuclei, this nonaxial mode will be neglected.

A typical example of PES on the  $(q_2, q_3)$  plane for  $^{184}\text{Hg}$ , where the macroscopic-microscopic energy of  $^{184}\text{Hg}$  is minimized with respect to the neck degree of freedom  $q_4$ , is shown in Fig. 2. The labels at the layers correspond to the energy (in MeV) with respect to the LSD macroscopic energy of spherical nucleus. The first saddle is noticed at  $q_2 = 1.28$  and  $q_3 = 0$ , while the second one is at  $q_2 = 1.69$  and  $q_3 = 0.03$ . Let us notice that this 2D energy map is only a projection of the full 3D PES onto  $(q_2, q_3)$  plane. A more complete PES structure of  $^{184}\text{Hg}$  can be observed in Fig. 3, where the  $(q_3, q_4)$  cross sections corresponding to different elongations  $q_2 = 2.0, 2.1, 2.2,$  and  $2.3$  are shown, respectively.

It can be seen that in Fig. 3 there are two competing minima, or better to say, fission valleys: one corresponding to the asymmetric fission around  $q_3 = 0.06$  and  $q_4 = 0$ , and the second one towards symmetric fission around  $q_3 = 0$  and  $q_4 = -0.15$ . One can also see that with increasing  $q_2$  the symmetric valley becomes deeper. The solid red lines marked in maps of Fig. 3 correspond to the liquid drop neck radius equaling to the nucleon radius, which roughly approximates the scission lines. Note that in the bottom map of Fig. 3, the red line, which begins at  $q_3 = 0, q_4 = -0.15$ , separates configurations belonging to the compact and the two-fragment shapes. Therefore for  $q_2 = 2.30$ , a significant part of the map refers to the noncompact configurations. Since our collective approach is destined for the compact system only, one truncates the collective space at  $q_2 = 2.30$ .

The probability distribution (7) for different mass numbers ( $A_f$ ) as a function of the elongation  $q_2$ , is shown in Fig. 4. It is seen that at deformations  $q_2 \leq 2.15$ , the asymmetric fission with the heavier fragment mass number  $A_f \approx 106$  is the most probable mode, while at larger elongations, the symmetric fission channel begins to dominate. The interplay between these different fission modes depends on the fission dynamics and the neck-break probability as described in the previous section. Similarly as in Ref. [6], the  $d$  parameter in Eq. (9) is adjusted to the known experimental FMD's [21,22], while

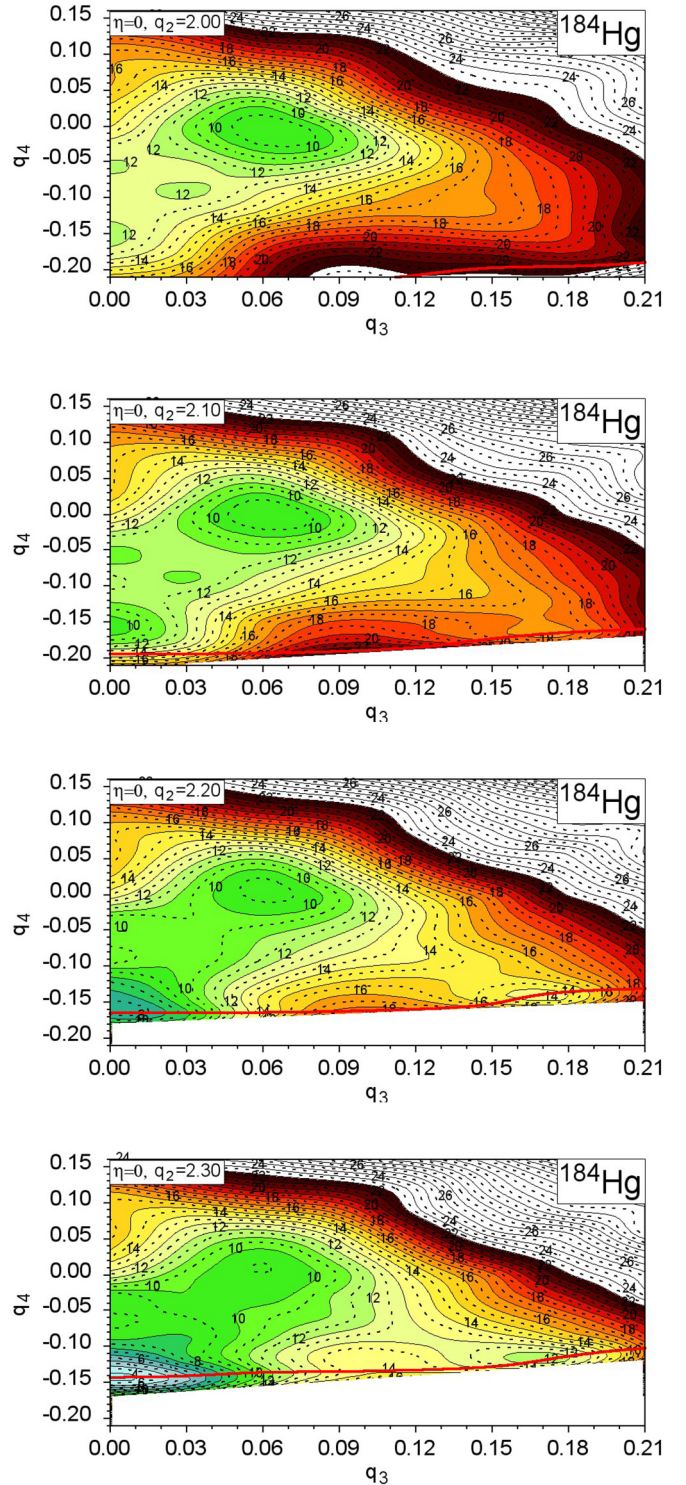


FIG. 3. Potential energy surface cross sections of  $^{184}\text{Hg}$  on the plane  $(q_3, q_4)$ . The panels from top to bottom correspond to elongations  $q_2 = 2.0, 2.1, 2.2,$  and  $2.3$ , respectively. The solid red lines drawn in each panel correspond to the neck radius equaling to the nucleon radius.

$E_0 = 1$  MeV (6) remains unchanged. In practice, it is found that when the geometrical probability factor  $P_{\text{neck}}$  is taken in the form of Fermi or Lorentz function, the FMD's are almost

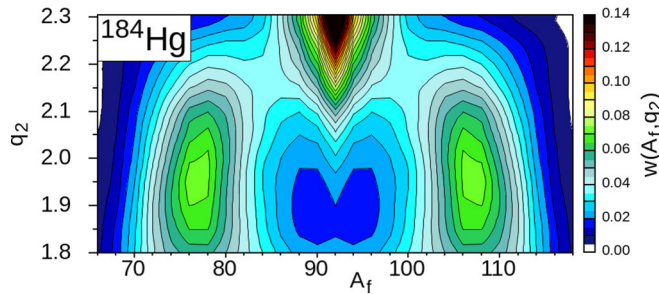


FIG. 4. Fission fragment distribution probability of  $^{184}\text{Hg}$  integrated over the deformation parameter  $q_4$  [see Eq. (7)] at the  $(A_f, q_2)$  plane.

independent of the half-width  $d$ , while if Gaussian function is used, the FMD's are much more sensitive with it. For  $d = 2.0$  fm, all the above-discussed forms of the neck-breaking probability functions lead to almost the same FMD's and the best agreements with the experimental data [21,22]. This value of the neck radius is in line with Ref. [1] in which one has assumed  $R_{\text{neck}} = 2.5$  fm at which one ends the random walk trajectories. Finally, the value of parameter  $d$  is fixed to 2.0 fm giving special weight to Hg isotopic chain, while  $d = 1.1$  fm for Pu nuclei in Ref. [6] was obtained for a slightly smaller size of the collective space. This difference may be also related to different geometrical features of fission barriers in these two regions. One can say that in the considered Pt-Ra isotopes, the parameter  $d$  tunes the interplay between the asymmetric and symmetric peaks in the FMD's. In fact,  $d$  can be adjusted for each isotopic chain separately. However, to maintain the predictive power of the present model, a unified value of  $d = 2$  fm is used for the whole lighter mass region.

In Fig. 5 we can see the FMD's of Pt-Hg isotopes. In the examined isotopic chains of even-even Pt nuclei, the FMD's gradually evolve from two-peak asymmetric division with a nonzero admixture of symmetric fission towards the division with dominating symmetric channel in the neutron-deficient isotopes. Moreover, the asymmetric channel strongly competes with the symmetric one in  $^{178-188}\text{Pt}$ , while the latter one is gradually suppressed in  $^{190-198}\text{Pt}$ .

Similar behaviors exhibit FMD in Hg (Fig. 5), Pb, and Po (Fig. 6) isotopes. For the three experimentally measured isotopes  $^{180-184}\text{Hg}$  [23–25], the theoretical FMD's asymmetric peaks are underestimated distinctly, however, their overall shapes are reproduced. Note that in contrary to the estimates made in Ref. [26], our model predicts the asymmetric fission to be the most probable mode in the lightest Hg isotopes. Our prediction for  $^{180}\text{Hg}$  is in line with the experimental data [23] and in addition is confirmed by Ref. [27], where the asymmetric fission mass distribution was deduced from total kinetic energy yield of the fragments. The asymmetric peaks in the FMD for  $^{182}\text{Hg}$  is less visible, because the measurement reported in Ref. [24] was performed at excitation energy  $E^* = 33.5$  MeV, which slightly suppressed the shell effect. A substantially better reproduction of measured mass divisions is observed in Po isotopes. For  $^{194}\text{Po}$  and  $^{196}\text{Po}$ , theoretical curves fit within the error bars of the experimental distributions taken from Ref. [21].

In Fig. 7, the predicted evolution of FMD's in Rn isotopic chains is completely opposite to the previously discussed Pt-Po even-even chains. Neutron-deficient  $^{196-204}\text{Rn}$  preferentially fission into two symmetric fragments, while in  $^{206-212}\text{Rn}$  an asymmetric component is getting more and more pronounced. The asymmetric peak becomes comparably high in moderately neutron-excessed  $^{214-218}\text{Rn}$ , while the symmetric peak in strongly neutron-rich  $^{222-226}\text{Rn}$  is suppressed significantly. In the experimentally measured  $^{202-208}\text{Rn}$  isotopes, the dominating symmetric divisions are reproduced with a tendency to slightly underestimate the asymmetric fission. Similar situations appear in Ra isotopes. The rather broad symmetric FMD's, which are found experimentally in  $^{210-218}\text{Ra}$ , is confronted with the rather narrow symmetric peaks and the smaller asymmetric bump around  $A_f = 126$ , which are predicted by our model. The dominating asymmetric fission with heavier mass fragment around  $A_f = 138$  is predicted to be heaviest for the investigated Ra isotopes. In the cases when the experimental FMD's are available as functions of the fragment charge ( $Z_f$ ), we have simply assumed that  $Z/A = Z_f/A_f$ , where  $Z$  and  $A$  are the charge and mass numbers of the mother nucleus, respectively.

It must be pointed out that the experimental FMD's in the above Rn and Ra isotopes correspond to their fission at  $E^* \approx 18$  MeV, i.e., about 10 MeV above the saddle point, which corresponds to the initial temperature of fissioning nucleus around  $T = 0.7$  MeV. At such temperature the pairing correlations in nuclei become weaker or even disappear, which could influence the width of symmetric and asymmetric valleys in the PES's. In addition, one has to remind that there is no dissipation in our model and it is known that this effect enlarges the width of the fission fragment yields.

#### IV. SUMMARY AND CONCLUSIONS

Summarizing our investigations we can write:

- (i) a three-dimensional set of the Fourier deformation parameters is sufficient to describe the properties of the fission process;
- (ii) potential energy surfaces of nuclei are evaluated in the macroscopic-microscopic model, where the LSD energy has been used for the macroscopic smooth part, while the shell and pairing corrections are estimated on the basis of the Yukawa-folded single-particle potential;
- (iii) a collective 3D model based on the elongation, mass asymmetry, and neck modes is introduced;
- (iv) a Wigner function is used to approximate the probability distribution related to the neck and mass asymmetry degrees of freedom;
- (v) a neck-breaking probability depending on the neck size is introduced in order to reproduce the measured fission fragment mass yields.

It is shown that our collective 3D model, which couples fission, neck, and mass asymmetry collective modes is able to describe the main features of the fragment mass yields in Pt-Ra and Pu isotopes. Due to its simplicity, this model

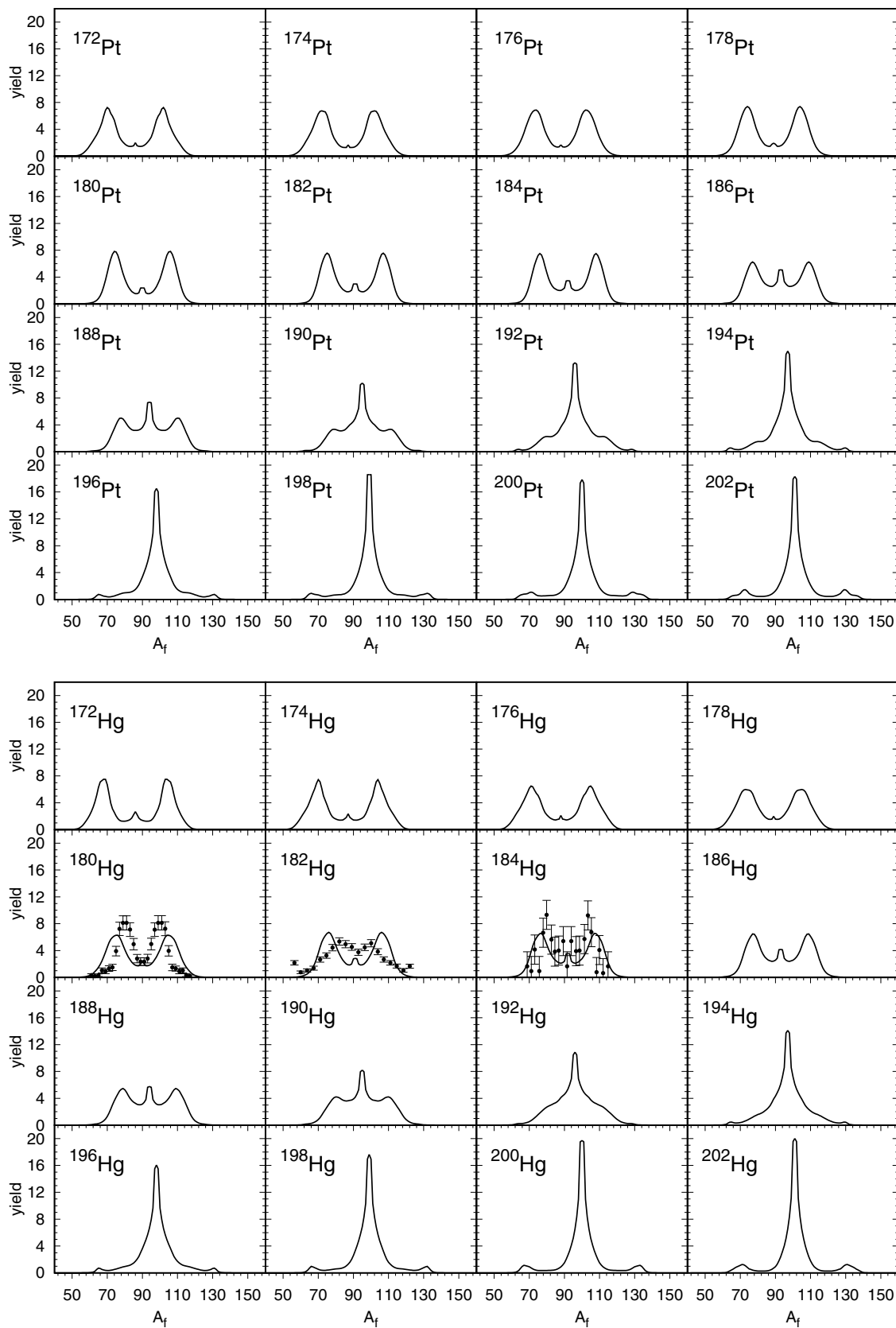


FIG. 5. Fission fragment mass yields of Pt (top) and Hg (bottom) isotopes. Experimental data (points with bars) are taken from Refs. [23–25].

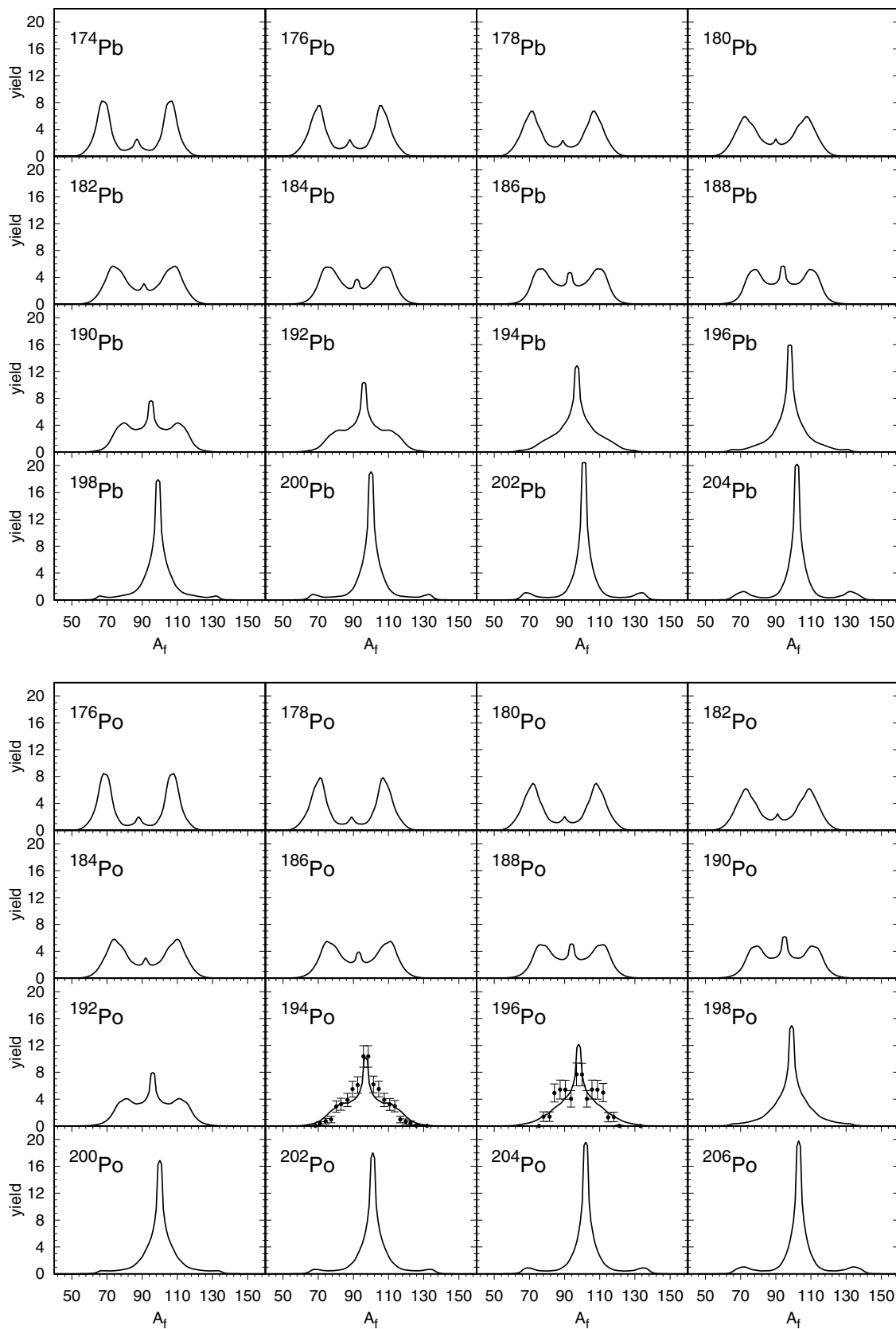


FIG. 6. Fission fragment mass yields of Pb (top) and Po (bottom) isotopes. Experimental data (points with bars) are taken from Ref. [21].



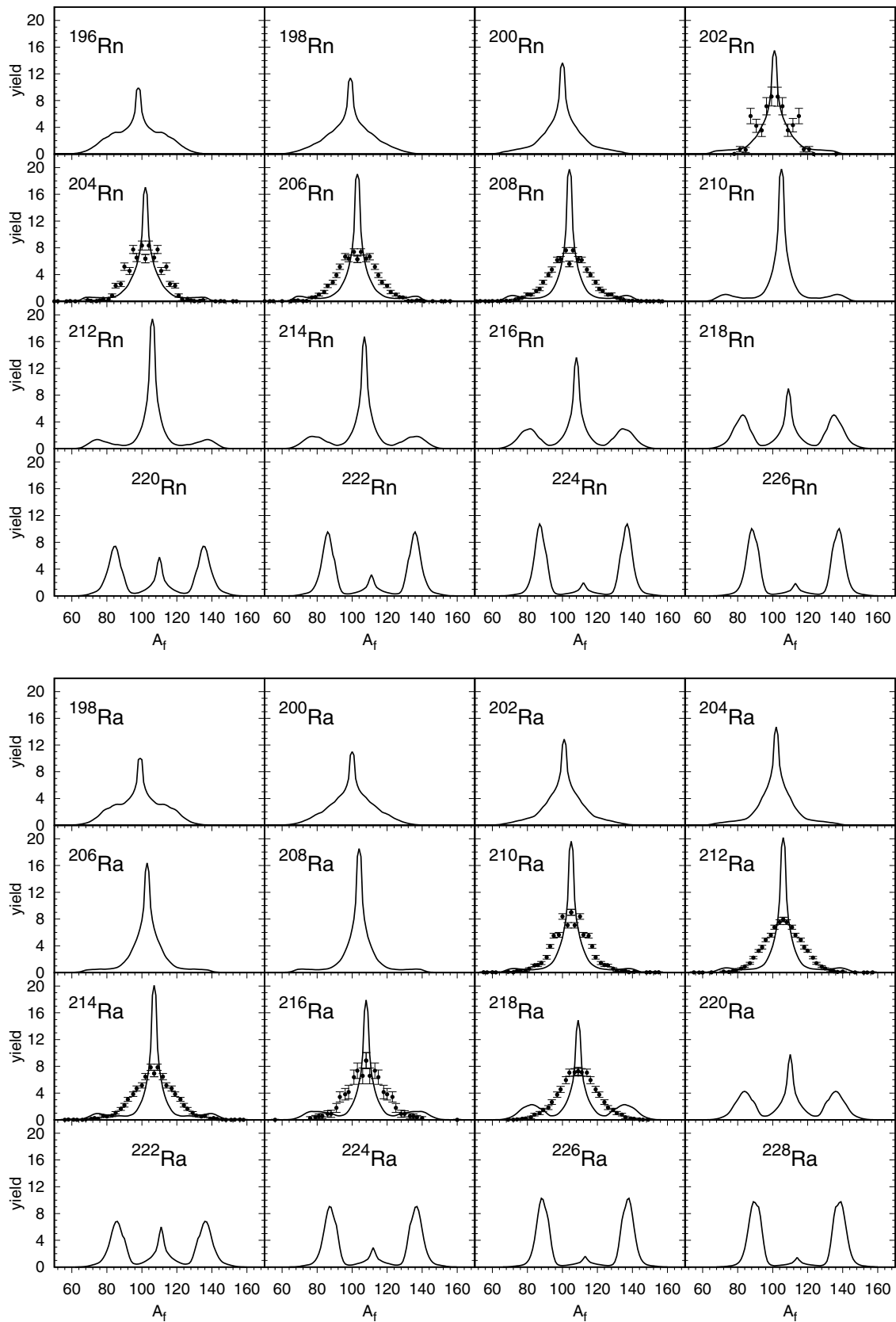


FIG. 7. Fission fragment mass yields of Rn (top) and Ra (bottom) isotopes. Experimental data (points with bars) are taken from Refs. [21,22,28].



may serve for the rapid and pilot-type calculations of fission properties. To obtain more precise results one has to use more advanced models in which the energy dissipation and particle evaporation are taken into account in the fission dynamics, e.g., the Langevin dynamics (Ref. [2]) or the improved quantum molecular dynamics model (ImQMD), which has been successfully applied to describe the fission process in the heavy-ion-induced fission reactions, where the excitation energy increases leading possibly to shorter fission time scale and even to the occurrence of a ternary fission [29–31]. Such calculations, based on the Fourier shape parametrization, as well as on the self-consistent method,

are planned to be carried out by our group in the close future.

#### ACKNOWLEDGMENTS

This work is supported by the Polish National Science Center (Grant No. 2018/30/Q/ST2/00185) and by the National Natural Science Foundation of China (Grant No. 11961131010), and the NSFC (Grants No. 11790325, No. 11875174, and No. 11890712). The authors would like to thank Christelle Schmitt for supplying us with a part of the experimental data.

- 
- [1] M. R. Mumpower, P. Jaffke, M. Verriere, and J. Randrup, *Phys. Rev. C* **101**, 054607 (2020).
- [2] H. J. Krappe and K. Pomorski, *Theory of Nuclear Fission*, Lecture Notes in Physics 838 (Springer-Verlag, Berlin, 2012).
- [3] B. Nerlo-Pomorska, K. Pomorski, and E. Werner, *International Conference on Fifty Years Research in Nuclear Fission*, Contributed Papers (Hahn-Meitner-Institut Berlin, Berlin, 1989), p. 63.
- [4] B. Nerlo-Pomorska, K. Pomorski, and F. A. Ivanyuk, *Acta Phys. Pol. B Suppl.* **8**, 659 (2015).
- [5] K. Pomorski, F. A. Ivanyuk, and B. Nerlo-Pomorska, *Eur. Phys. J. A* **53**, 59 (2017).
- [6] K. Pomorski, B. Nerlo-Pomorska, J. Bartel, and C. Schmitt, *Eur. Phys. J. Web Conf.* **169**, 00016 (2018).
- [7] K. Pomorski and J. Dudek, *Phys. Rev. C* **67**, 044316 (2003).
- [8] K. T. R. Davies and J. R. Nix, *Phys. Rev. C* **14**, 1977 (1976).
- [9] A. Dobrowolski, K. Pomorski, and J. Bartel, *Comput. Phys. Commun.* **199**, 118 (2016).
- [10] K. Pomorski, B. Nerlo-Pomorska, J. Bartel, and C. Schmitt, *Acta Phys. Pol. B Suppl.* **8**, 667 (2015).
- [11] C. Schmitt, K. Pomorski, B. Nerlo-Pomorska, and J. Bartel, *Phys. Rev. C* **95**, 034612 (2017).
- [12] J. Bartel, K. Pomorski, B. Nerlo-Pomorska, and H. Molique [Acta Phys. Pol. B Supl. (to be published)].
- [13] M. Brack, J. Damgaard, A. S. Jensen, H. C. Pauli, V. M. Strutinsky, and C. Y. Wong, *Rev. Mod. Phys.* **44**, 320 (1972).
- [14] V. M. Strutinsky, *Sov. J. Nucl. Phys.* **3**, 449 (1966); *Nucl. Phys. A* **95**, 420 (1967); **122**, 1 (1968).
- [15] S. G. Nilsson, C. F. Tsang, A. Sobiczewski, Z. Szymański, S. Wycech, S. Gustafson, I. L. Lamm, P. Möller, and B. Nilsson, *Nucl. Phys. A* **131**, 1 (1969).
- [16] J. Bardeen, L. N. Cooper, and J. R. Schrieffer, *Phys. Rev.* **108**, 1175 (1957).
- [17] A. Góźdz and K. Pomorski, *Nucl. Phys. A* **451**, 1 (1986).
- [18] S. Piłat, K. Pomorski, and A. Staszczak, *Z. Phys. A* **332**, 259 (1989).
- [19] J. Randrup, S. E. Larsson, P. Möller, S. G. Nilsson, K. Pomorski, and A. Sobiczewski, *Phys. Rev. C* **13**, 229 (1976).
- [20] L. Dematté, C. Wagemans, R. Barthélémy, P. D’hondt, and A. Deruytter, *Nucl. Phys. A* **617**, 331 (1997).
- [21] C. Ghys *et al.*, *Phys. Rev. C* **90**, 041301(R) (2014).
- [22] K.-H. Schmidt *et al.*, *Nucl. Phys. A* **665**, 221 (2000); **693**, 169 (2001).
- [23] J. Elseviers *et al.*, *Phys. Rev. C* **88**, 044321 (2013).
- [24] E. Prasad *et al.*, *Phys. Rev. C* **91**, 064605 (2015).
- [25] T. Gorbinet and SOFIA Collaboration, 10th ASRC Int. Workshop on “Nuclear Fission and Decay of Exotic Nuclei”, JAEA, March 22, 2013.
- [26] A. V. Andreev, G. G. Adamian, N. V. Antonenko, and A. N. Andreyev, *Phys. Rev. C* **88**, 047604 (2013).
- [27] V. Liberati *et al.*, *Phys. Rev. C* **88**, 044322 (2013).
- [28] J. Randrup and P. Möller, *Phys. Rev. C* **88**, 064606 (2013).
- [29] Q. H. Wu, X. Y. Diao, F. H. Guan, Y. J. Wang, Y. X. Zhang, Z. X. Li, X. Z. Wu, K. Pomorski, and Z. G. Xiao, *Phys. Lett. B* **797**, 134808 (2019).
- [30] J. L. Tian, X. Z. Wu, Z. X. Li, K. Zhao, Y. Zhang, X. Li, and S. Yan, *Phys. Rev. C* **82**, 054608 (2010).
- [31] C. Li, J. L. Tian, Y. J. Qin, J. J. Li, and N. Wang, *Chin. Phys. C* **37**, 114101 (2013).